Nonlinear regional warming with increasing CO_2 concentration

Article

Nonlinear regional warming at higher CO_2 concentrations

Peter Good[1], Jason A. Lowe[1], Timothy Andrews[1], Andrew Wiltshire[1], Robin Chadwick[1], Jeff K Ridley[1], Matthew B Menary[1], Nathaelle Bouttes[2], Jean Louis Dufresne[3], Jonathan M Gregory[2,1], Nathalie Schaller[4,5], Hideo Shiogama[6]

[1] Met Office Hadley Centre, Exeter, United Kingdom

[2] NCAS-Climate, University of Reading, Reading, United Kingdom

[3] Laboratoire de Météorologie Dynamique, Institut Pierre Simon Laplace, Paris,France

[4] Institute for Atmospheric and Climate Science, Department of Environmental Sciences, Swiss Federal Institute of Technology, Zurich, Switzerland

[5] Atmospheric, Oceanic and Planetary Physics, University of Oxford, Parks Road, Oxford OX1 3PU, United Kingdom

[6] Climate Risk Assessment Section, Centre for Global Environmental Research, National Institute for Environmental Studies, Tsukuba, Japan

To be submitted to Nature Climate Change

Contact information (corresponding author with asterisk)

peter.good@metoffice.gov.uk*

jason.lowe@metoffice.gov.uk
timothy.andrews@metoffice.gov.uk
andy.wiltshire@metoffice.gov.uk
robin.chadwick@metoffice.gov.uk
jeff.ridley@metoffice.gov.uk
matthew.menary@metoffice.gov.uk
n.bouttes@reading.ac.uk
Jean-Louis.Dufresne@lmd.jussieu.fr
j.m.gregory@reading.ac.uk
Schaller@atm.ox.ac.uk
shiogama.hideo@nies.go.jp

In the debate on acceptable levels of climate change, and for planning adaptation measures, stakeholders need regional-scale climate projections including the range of plausible warming rates. To assess the benefits of mitigation, it is important to understand whether some locations may see disproportionately high or low warming from additional forcing above targets such as 2 K[1]. There is an urgent need to narrow uncertainty[2] in this nonlinear warming, which requires understanding how climate changes as forcings increase from medium to high levels. However, quantifying and understanding regional nonlinear processes is challenging. Here we show that regional-scale warming can be strongly super-linear to successive CO_2 doublings, using five different climate models. Ensemble-mean warming is super-linear over most land locations. Further, the inter-model spread tends to be amplified at higher forcing levels, as nonlinearities grow – especially when considering changes per K of global warming. Regional nonlinearities in surface warming arise from nonlinearities in global-mean radiative balance, the Atlantic Meridional Overturning Circulation, surface snow/ice cover and evapotranspiration. In quantifying and understanding the benefits of mitigation, potentially-avoidable climate change (the difference between business-as-usual and mitigation scenarios) and unavoidable climate change (change under strong mitigation scenarios) may need different treatments.

Linear assumptions affect stakeholder advice in various ways[1,3-7]. Fast simplified models[1,5,7] (especially integrated assessment models), for quantifying climate change under many policy scenarios, often assume climate change is the same for each CO_2 doubling. Some studies make a less strong assumption: that regional climate is linear in global warming[3,4,6]. Also, studies of physical mechanisms often explore just one time period of one forcing scenario. An implied linear assumption here is that the

64 physical mechanisms are similar under other scenarios or for other time periods (not
65 necessarily true in a nonlinear system).
66
67 To quantify nonlinearities, the linear response must first be carefully defined. Even in
68 a linear system the spatial patterns of climate change (per CO_2 doubling or per K of
69 global warming) can be different in different forcing scenarios or evolve during a
70 given scenario. This is because of different timescales of response within a system[8-
71 10]. For example, warming over the Southern Ocean lags the global mean[10]. Therefore,
72 the spatial pattern of warming just after a CO_2 change is different than that several
73 decades later.
74
75 Our experimental design is chosen to separate linear and nonlinear mechanisms. We
76 use abruptCO_2 experiments, initialized from a pre-industrial control experiment. The
77 CO_2 concentration is changed abruptly, then held constant for 150 years, revealing the
78 model response over different timescales. The abrupt4xCO_2 experiment (with CO_2
79 quadrupled from pre-industrial levels) has similar forcing magnitude as a business-as-
80 usual scenario by 2100[11]. The abrupt2xCO_2 experiment is identical to abrupt4xCO_2
81 but with half the CO_2 concentration (with forcing between that reached under RCP2.6
82 and RCP4.5 scenarios by year 2100[11]). A transient forcing experiment ('1pctCO_2'),
83 where CO_2 is increased by 1% per year, is also used. We start with results from the
84 HadGEM2-ES climate model.
85
86 The abruptCO_2 experiments are highly idealised. Therefore, we first show that their
87 behaviour is comparable to the more policy-relevant 1pctCO_2 experiment, and detect
88 nonlinearities in the 1pctCO_2 response. It is possible to use a simple linear

89 combination of abruptCO_2 responses to estimate climate change under a transient
90 forcing experiment[12,13]. This linear method performs well when the end of the
91 1pctCO_2 experiment (near 4xCO_2) is reconstructed from the abrupt4xCO_2 response
92 (Figure 1b). This shows that the abrupt4xCO_2 experiment features realistic physical
93 mechanisms. It does not mean that temperature responses are linear (conceptually, it
94 is like a local linear approximation to a curve). The importance of nonlinearity is
95 revealed in the relatively poor performance when the abrupt2xCO_2 response is used
96 instead (Figure 1a); while for the middle of 1pctCO_2 (near 2xCO_2), the reconstruction
97 using abrupt4xCO_2 is much worse than that using abrupt2xCO_2 (compare Figures
98 1c,d). The linear method is only accurate for periods in the transient experiment with
99 forcing matching that of the abruptCO_2 experiment: climate patterns are therefore
100 different for different CO_2 concentrations – which is evidence of nonlinearity.
101
102 Having detected nonlinearities in the 1pctCO_2 experiment, we characterise them more
103 clearly by analysing the abruptCO_2 experiments directly. This experimental design
104 has two significant advantages over the 1pctCO_2 scenario. First, temperature
105 responses in the two abruptCO_2 experiments may be compared at the same timescale
106 after CO_2 is changed (eliminating complications due to linear effects from different
107 timescales of response). Secondly, noise from internal variability may be reduced
108 through long-term means. Assuming that the balance of mechanisms should be stable
109 after the initial ocean mixed-layer warming, we average over years 50-149 of each
110 experiment (Supplementary Figure 1). For abrupt2xCO2, these 100-year means
111 correspond roughly to the results for year 2100 of a CO2-only version of rcp4.5 (and
112 about double this for abrupt4xCO2).
113

We compare temperature responses to a first and second CO_2 doubling. Current linear methods that parameterise forcing (most integrated assessment and energy balance models) assume that radiative forcing is exactly linear in log(CO2) – and equivalently, that each CO2 doubling produces the same forcing change[1,5]. In HadGEM2-ES, the two doublings give very similar forcing changes[14]. The response to the first doubling is given by abrupt2xCO_2 minus the pre-industrial control; that for the second doubling by abrupt4xCO_2 minus abrupt2xCO_2 (both are averaged over years 50-149). We quantify nonlinearities by the 'doubling difference': the response to the second doubling minus that for the first (Figure 2a); and the 'doubling ratio': the second doubling divided by the first (Figure 2b). Current linear models would have zero doubling difference everywhere.

The doubling ratio in global-mean warming is 1.18 (the second CO_2 doubling produces more warming than the first). Global-scale nonlinearity has been attributed, in other models, to changes in water-vapor and cloud feedbacks, opposed by changes in albedo and lapse-rate feedbacks[15-17]. In some climate models, variation in forcing per CO_2 doubling would also affect the global doubling ratio[15-17]. Regional variation in doubling ratio is broad, however: 5% of the land surface has a doubling ratio outside the range 0.9-1.65 (Supplementary Figure 5a). Gradients of the doubling ratio across continents are strong (Figure 2b), notably over the Americas and Europe, pointing to important regional mechanisms.

We scale out global-mean nonlinearity (Methods) and then focus on the remaining features (see Figure 2c) one by one. The positive area in the north Atlantic, near Greenland, appears to be associated with a nonlinear response of the Atlantic

Meridional Overturning Circulation (AMOC)[18]. In HadGEM2-ES, the maximum Atlantic overturning near 30N weakens about 35% less under a second CO_2 doubling than under the first (a positive doubling difference). We can estimate the effect on surface temperature by scaling the regional temperature response in a separate freshwater hosing experiment (where freshwater is added to the high-latitude north Atlantic to induce AMOC weakening). We multiplied this temperature response pattern by the ratio: (doubling difference for AMOC index) / (AMOC index response in the hosing experiment). The resulting pattern (Figure 2d) features a north Atlantic anomaly similar to that in Figure 2c. This suggests that the north Atlantic nonlinearity is indeed driven by the nonlinear AMOC response. AMOC nonlinearity may arise from variation in the salt-advection feedback (which affects the AMOC strength)[19]. The AMOC transports heat to the North Atlantic, so a positive doubling difference in the AMOC causes positive doubling differences in North Atlantic surface temperatures.

To reveal other nonlinear mechanisms, we subtract the AMOC pattern (Figure 2d) from that in Figure 2c. The residual (Figure 2e) is associated with mechanisms other than those in the global mean energy balance or the AMOC. The North Atlantic positive feature has been effectively removed.

The remaining high-latitude temperature nonlinearities are largely driven by a nonlinear albedo feedback[18,20] (which is dominated by changes in ice and snow cover). It is nonlinear[21] as it becomes zero when ice/snow is either absent or so thick that its extent changes little under warming. The patterns in the doubling difference of sea ice fraction (Figure 2f) match closely the high latitude patterns of temperature doubling

164 difference (Figure 2e), with sea-ice albedo feedbacks driving temperature nonlinearity
165 (supplementary material).
166
167 The final mechanism we study involves land evapotranspiration. Soil moisture-
168 temperature feedbacks can be nonlinear[22]: feedback is small when soil moisture is
169 saturated, or so low that moisture is tightly bound to the soil (in both regimes,
170 evaporation is insensitive to change in soil moisture)[23]. Nonlinear behaviour could
171 also occur through the response of plant stomata (and hence transpiration) to
172 increased CO_2[24], or through nonlinear precipitation change[25,26]. To investigate this
173 type of effect, we calculate the ratio of mean surface sensible heat and mean surface
174 latent heat fluxes (the Bowen ratio) in the two abruptCO_2 experiments. Much of the
175 temperature nonlinearity over mid/low latitude land (Figure 2g) is associated with
176 change in the Bowen ratio (see Figure 2h). Regions where the Bowen ratio is
177 substantially larger at 4xCO_2 than at 2xCO_2 (red in Figure 2h) have more restricted
178 evaporation: more incident heat is lost as sensible heat, causing further warming. This
179 does not occur where the Bowen ratio is already larger than 1 at 2xCO_2 (e.g. the
180 Sahara, where most turbulent heat is sensible even at 2xCO_2). These regions are
181 masked in Figure 2h. The most strongly superlinear warming occurs over the
182 Amazon in this model (doubling ratios of 80% are driven by the response of forest
183 tree stomata to CO_2, with a longer-term response from reduced vegetation
184 productivity - supplementary material; these mechanisms are highly uncertain).
185
186 Further to our analysis of HadGEM2-ES we find that nonlinearity is similarly
187 important in four other climate models: NCAR-CESM1, IPSL CM5A-LR, MIROC5
188 T42 and HadCM3. These models show doubling ratios over land comparable to those

189 in HadGEM2-ES (supplementary Figure 5a). Over most land locations, the ensemble
190 mean doubling difference is comparable to the ensemble standard deviation for
191 warming from the first doubling (supplementary Figure 5b). That is, the range of
192 warmings simulated by this ensemble is quite different for the first and second CO_2
193 doublings. The models do show differences in spatial patterns of nonlinear warming.
194 Consequently, the ensemble mean pattern (Figure 3) is smoother than that of any
195 individual model. However, some continental-scale patterns across Europe, North
196 and South America and tropical Africa are similar between Figures 2b and 3.
197
198 Nonlinearity has implications not just for the ensemble mean, but also for the spread
199 of model projections. In general, an increased spread at higher forcing should be
200 expected: the relative importance of nonlinear mechanisms grows with increasing
201 forcing, so their contribution to model spread does likewise. Conceptually, this is like
202 including an extra uncertain process at higher CO_2 concentrations. This inflation in
203 model spread at higher forcing is large when nonlinearities are uncertain
204 (supplementary material), and appears to be especially relevant for change per K of
205 global warming. We calculated the ensemble standard deviation in regional warming
206 per K of global warming. Over 30% of land, the ensemble spread is at least 40%
207 larger for the second doubling than for the first doubling (not driven by internal
208 variability – Supplementary Material). This corresponds to a doubling of variance -
209 driven by uncertain nonlinear mechanisms. This finding is important for work
210 quantifying and reducing model uncertainty. It implies that the additional regional
211 warming under a business-as-usual scenario (over and above that in a mitigation
212 scenario) may be more uncertain than the warming under a mitigation scenario - a fact
213 missed by previous linear impacts assessments[1,3,4]. Secondly, different techniques

may be needed to reduce model uncertainty in these two aspects of climate change: uncertainty from nonlinear mechanisms being relatively more important at higher than at lower forcing levels.

The mechanisms of nonlinear warming identified in HadGEM2-ES also operate in the other four models studied. All have a positive global-mean temperature nonlinearity (Supplementary Table 1). As done for HadGEM2-ES, we scale this global-mean nonlinearity out and discuss regional patterns. Most of the remaining temperature nonlinearities over North-West Europe are associated with the AMOC: the magnitude of this nonlinearity is predicted simply by scaling the HadGEM2-ES hosing experiment by the AMOC doubling difference from each model (Figure 4a). While there is significant model spread in sea-ice nonlinearity (Supplementary Figure 6), Arctic temperature doubling differences averaged across the four extra models align closely with the sea-ice albedo doubling differences (Figure 4b,c), with patterns similar to those for HadGEM2-ES (Figure 2f). Similar comments apply to the evaporation mechanism at lower latitudes (Figure 4d,e; Supplementary Figure 7), especially over the Americas, Africa and Arabia, although not all of the pattern is explained this way (nonlinear dynamical processes and internal variability may also contribute).

The implications of nonlinearity for individual studies will be application-specific, and should be considered alongside other issues, such as impacts model uncertainty. Further differences in patterns of 'potentially-avoidable' and 'unavoidable' warming may arise from linear mechanisms. The abruptCO2 experiments are powerful for separating mechanisms and identifying where nonlinearity is largest or smallest.

Where available, transient projections from state-of-the-art climate models remain preferable for direct policy advice.

Work is needed to reduce uncertainty in these nonlinear mechanisms. Our experimental design could usefully be applied to other models. Some policy advice based on linear methods[3] may need to be reconsidered, while studies of physical processes controlling both temperature and precipitation[25,26] should account for a different balance of mechanisms under different forcing scenarios or for different time periods.

Methods

HadGEM2-ES model and experiments

The Hadley Centre Global Environmental Model version 2 Earth System configuration (HadGEM2-ES) [27,28] has an atmospheric resolution of 1.25x1.875^{o} and 38 vertical levels, and a 1^{o} ocean (reaching 1/3^{o} near the equator) with 40 vertical levels. NCAR CESM1, HadCM3, IPSL CM5A-LR and MIROC5 are described in supplementary Table 2.

All models ran a fixed-forcings pre-industrial control, and both abruptCO_2 experiments. Each abruptCO_2 experiment was initialised from the same point in the control run, and CO_2 was abruptly changed (to twice pre-industrial levels for abrupt2xCO_2 and four times for abrupt4xCO_2), and then held constant for 150 years.

The hosing experiment, run for HadGEM2-ES only, involved addition of 0.1Sv freshwater near the coast of Greenland for 100 years. This produced a modest (30%) slowdown in the AMOC (measured by maximum overturning near 30N). Results from this experiment were averaged over years 50-149.

Scaling the global-mean nonlinearity out of the regional temperature doubling differences

Figure 2c shows doubling differences after the global-mean nonlinearities (except those due to the AMOC) are scaled out. The calculation of doubling differences with global non-linearities scaled out (denoted $DD_{noglobal}$) is described below. The small global-mean nonlinearity associated with the AMOC is not scaled out here. This is because the global-mean AMOC effect is included in Figure 2d (the scaled hosing response), and is therefore removed when Figure 2d is subtracted from Figure 2c: to give the residual in Figure 2e. $DD_{noglobal}$ is given by:

$$DD_{noglobal} = T_{42} - T_{21,scaled}$$

where T_{42} is the warming from the second doubling, and:

$$T_{21,scaled} = T_{21} \cdot \frac{\left(\overline{T_{21}} + \overline{DD_{noAMOC}}\right)}{\overline{T_{21}}}$$

where T_{21} is the warming from the first doubling. The overbar indicates a global

mean. $\overline{DD_{noAMOC}}$ is the global mean doubling difference from processes other than the AMOC:

$$\overline{DD_{noAMOC}} = \overline{DD} - \overline{DD_{AMOC}}$$

$\overline{DD}$ is the global mean of Figure 2a and DD_{AMOC} is the global mean of Figure 2d.

References

1 Arnell, N. W. *et al.* A global assessment of the effects of climate policy on the impacts of climate change. *Nat Clim Change* **3**, 512-519, doi:Doi 10.1038/Nclimate1793 (2013).

2 Oppenheimer, M. Defining dangerous anthropogenic interference: The role of science, the limits of science. *Risk Anal* **25**, 1399-1407, doi:DOI 10.1111/j.1539-6925.2005.00687.x (2005).

3 Gosling, S. N. *et al.* A review of recent developments in climate change science. Part II: The global-scale impacts of climate change. *Prog Phys Geog* **35**, 443-464, doi:Doi 10.1177/0309133311407650 (2011).

4 Todd, M. C. *et al.* Uncertainty in climate change impacts on basin-scale freshwater resources - preface to the special issue: the QUEST-GSI methodology and synthesis of results. *Hydrol Earth Syst Sc* **15**, 1035-1046, doi:DOI 10.5194/hess-15-1035-2011 (2011).

5 van Vuuren, D. P. *et al.* How well do integrated assessment models simulate climate change? *Climatic Change* **104**, 255-285, doi:DOI 10.1007/s10584-009-9764-2 (2011).

6 Moss, R. H. *et al.* The next generation of scenarios for climate change research and assessment. *Nature* **463**, 747-756, doi:Doi 10.1038/Nature08823 (2010).

7 Huntingford, C. *et al.* Simulated resilience of tropical rainforests to CO2-induced climate change. *Nat Geosci* **6**, 268-273, doi:Doi 10.1038/Ngeo1741 (2013).

8 Chadwick, R., Wu, P. L., Good, P. & Andrews, T. Asymmetries in tropical rainfall and circulation patterns in idealised CO2 removal experiments. *Climate Dynamics* **40**, 295-316, doi:DOI 10.1007/s00382-012-1287-2 (2013).

9 Li, S. & Jarvis, A. Long run surface temperature dynamics of an A-OGCM: the HadCM3 4xCO(2) forcing experiment revisited. *Climate Dynamics* **33**, 817-825, doi:10.1007/s00382-009-0581-0 (2009).

10 Manabe, S., Bryan, K. & Spelman, M. J. Transient-Response of a Global Ocean Atmosphere Model to a Doubling of Atmospheric Carbon-Dioxide. *J Phys Oceanogr* **20**, 722-749, doi:Doi 10.1175/1520-0485(1990)020<0722:Troago>2.0.Co;2 (1990).

11 Meinshausen, M. *et al.* The RCP greenhouse gas concentrations and their extensions from 1765 to 2300. *Climatic Change* **109**, 213-241, doi:DOI 10.1007/s10584-011-0156-z (2011).

12 Good, P., Gregory, J. M. & Lowe, J. A. A step-response simple climate model to reconstruct and interpret AOGCM projections. *Geophysical Research Letters* **38**, -, doi:Artn L01703 Doi 10.1029/2010gl045208 (2011).

13 Good, P., Gregory, J. M., Lowe, J. A. & Andrews, T. Abrupt CO2 experiments as tools for predicting and understanding CMIP5 representative concentration pathway projections. *Climate Dynamics* **40**, 1041-1053, doi:DOI 10.1007/s00382-012-1410-4 (2013).

14 Andrews, T. & Ringer, M. A. Cloud Feedbacks, Rapid Adjustments, and the Forcing-Response Relationship in a Transient CO2 Reversibility Scenario. *Journal of Climate* **27**, 1799-1818, doi:Doi 10.1175/Jcli-D-13-00421.1 (2014).

15 Jonko, A. K., Shell, K. M., Sanderson, B. M. & Danabasoglu, G. Climate Feedbacks in CCSM3 under Changing CO2 Forcing. Part II: Variation of Climate Feedbacks and Sensitivity with Forcing. *Journal of Climate* **26**, 2784-2795, doi:Doi 10.1175/Jcli-D-12-00479.1 (2013).
16 Colman, R. & McAvaney, B. Climate feedbacks under a very broad range of forcing. *Geophysical Research Letters* **36**, doi:L01702 10.1029/2008gl036268 (2009).
17 Hansen, J. *et al.* Efficacy of climate forcings. *Journal of Geophysical Research-Atmospheres* **110**, 45, doi:D18104 10.1029/2005jd005776 (2005).
18 Ishizaki, Y. *et al.* Temperature scaling pattern dependence on representative concentration pathway emission scenarios. *Climatic Change* **112**, 535-546, doi:DOI 10.1007/s10584-012-0430-8 (2012).
19 Drijfhout, S. S., Weber, S. L. & van der Swaluw, E. The stability of the MOC as diagnosed from model projections for pre-industrial, present and future climates. *Climate Dynamics* **37**, 1575-1586, doi:DOI 10.1007/s00382-010-0930-z (2011).
20 Hall, A. The role of surface albedo feedback in climate. *Journal of Climate* **17**, 1550-1568, doi:Doi 10.1175/1520-0442(2004)017<1550:Trosaf>2.0.Co;2 (2004).
21 Eisenman, I. Factors controlling the bifurcation structure of sea ice retreat. *Journal of Geophysical Research-Atmospheres* **117**, doi:Artn D01111 Doi 10.1029/2011jd016164 (2012).
22 Seneviratne, S. I. *et al.* Investigating soil moisture-climate interactions in a changing climate: A review. *Earth-Sci Rev* **99**, 125-161, doi:DOI 10.1016/j.earscirev.2010.02.004 (2010).
23 Seneviratne, S. I., Luthi, D., Litschi, M. & Schar, C. Land-atmosphere coupling and climate change in Europe. *Nature* **443**, 205-209, doi:Doi 10.1038/Nature05095 (2006).
24 Field, C. B., Jackson, R. B. & Mooney, H. A. Stomatal Responses to Increased Co2 - Implications from the Plant to the Global-Scale. *Plant Cell Environ* **18**, 1214-1225, doi:DOI 10.1111/j.1365-3040.1995.tb00630.x (1995).
25 Chadwick, R. & Good, P. Understanding non-linear tropical precipitation responses to CO2 forcing. *Geophysical Research Letters* **40**, doi:10.1002/grl.50932 (2013).
26 Good, P. *et al.* A step-response approach for predicting and understanding non-linear precipitation changes. *Climate Dynamics* **39**, 2789-2803, doi:DOI 10.1007/s00382-012-1571-1 (2012).
27 Collins, W. J. *et al.* Development and evaluation of an Earth-System model – HadGEM2. *Geophysical Model Development (submitted)* (2011).
28 Martin, G. M. *et al.* The HadGEM2 family of Met Office Unified Model climate configurations. *Geosci Model Dev* **4**, 723-757, doi:DOI 10.5194/gmd-4-723-2011 (2011).

Acknowledgements

This work was supported by the Joint UK DECC/Defra Met Office Hadley Centre Climate Programme (GA01101). NB and JMG received funding from the European Research Council under the European Community's Seventh Framework Programme (FP7/2007-2013), ERC Grant Agreement 247220, project "Seachange." Simulations by J.L.D. were done as part of the ANR ClimaConf project (grant #ANR-10-CEPL-0003). HS was supported by the SOUSEI program from the Ministry of Education, Culture, Sports, Science and Technology of Japan and the Environment Research and Technology Development Fund (S-10) of the Ministry of the Environment of Japan. NS was supported by the Swiss National Science Foundation.

Author contributions

P.G. conceived the study and wrote the paper. All authors contributed to the scientific interpretation and the paper. T.A., M.B.M, J.L.D., J.M.G., N.S. and H.S. performed experiments.

Competing financial interests statement

The authors have no competing interests as defined by Nature Publishing Group, or other interests that might be perceived to influence the results and/or discussion reported in this article.

Figure legends

Figure 1. Regional nonlinearity in the transient-forced 1pctCO_2 experiment. Warming (K) simulated directly by HadGEM2-ES (y-axis) is compared with that predicted from the linear reconstruction[12,13] using (left column) abrupt2xCO_2 and (right column) abrupt4xCO_2 responses. Good performance of the linear reconstruction is indicated by the points lying close to the red line (each point represents one model grid cell). Results are averaged over (top row) years 120-139 of the 1pctCO_2 experiment (near 4xCO_2), and (bottom row) years 61-80 (near 2xCO_2).

Figure 2. Mechanisms of nonlinear regional warming in HadGEM2-ES. Left column: doubling differences (K); a) unscaled; c) after global-mean nonlinearity is scaled out (Methods); e) as c), but with nonlinearity associated with the AMOC (panel d) subtracted; g) as e) but latitude range matches that of panel h). b) doubling ratio. d) estimated nonlinearity associated with the AMOC. f) doubling difference in sea ice fraction. h) Bowen ratio at 4xCO_2 divided by Bowen ratio at 2xCO_2. All based on means over years 50-149 of the abrupt2xCO2, abrupt4xCO_2 or hosing experiments.

Figure 3. Doubling ratio of ensemble mean warming. Ensemble means are taken for each of the first and second CO_2 doublings first, then the doubling ratio calculated.

Figure 4. Multi-model mechanisms of temperature nonlinearity. All panels: 'scaled temperature doubling differences' have had the global mean nonlinearity scaled out**.** a) AMOC influence, averaged over NW Europe (land, 10W-20E, 45-70N). Y-axis: scaled temperature doubling difference for each model; x-axis: the HadGEM2-ES

hosing temperature response scaled using the doubling difference in AMOC index for each model (as Figure 2d; Pink: HadGEM2-ES; dark blue: HadCM3; light blue: MIROC5; yellow: NCAR CESM1; red: IPSL CM5A-LR). b,c) Sea-ice influence. Ensemble means (excluding HadGEM2), of b: scaled temperature doubling difference and c: albedo doubling difference. d,e) Evaporation influence. d: Ensemble mean (excluding HadGEM2) scaled temperature doubling difference; e: Bowen ratio of ensemble mean surface heat fluxes at $4xCO_2$, divided by the equivalent at $2xCO_2$ (as Figure 2h).

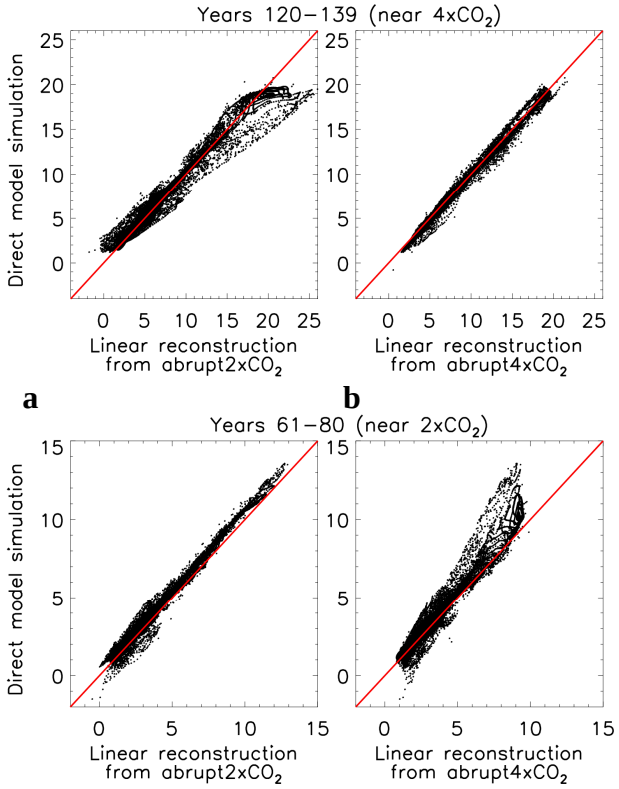

Figure 1. Regional nonlinearity in the transient-forced 1pctCO_2 experiment. Warming (K) simulated directly by HadGEM2-ES (y-axis) is compared with that predicted from the linear reconstruction[12,13] using (left column) abrupt2xCO_2 and (right column) abrupt4xCO_2 responses. Good performance of the linear reconstruction is indicated by the points lying close to the red line (each point represents one model grid cell). Results are averaged over (top row) years 120-139 of the 1pctCO_2 experiment (near 4xCO_2), and (bottom row) years 61-80 (near 2xCO_2).

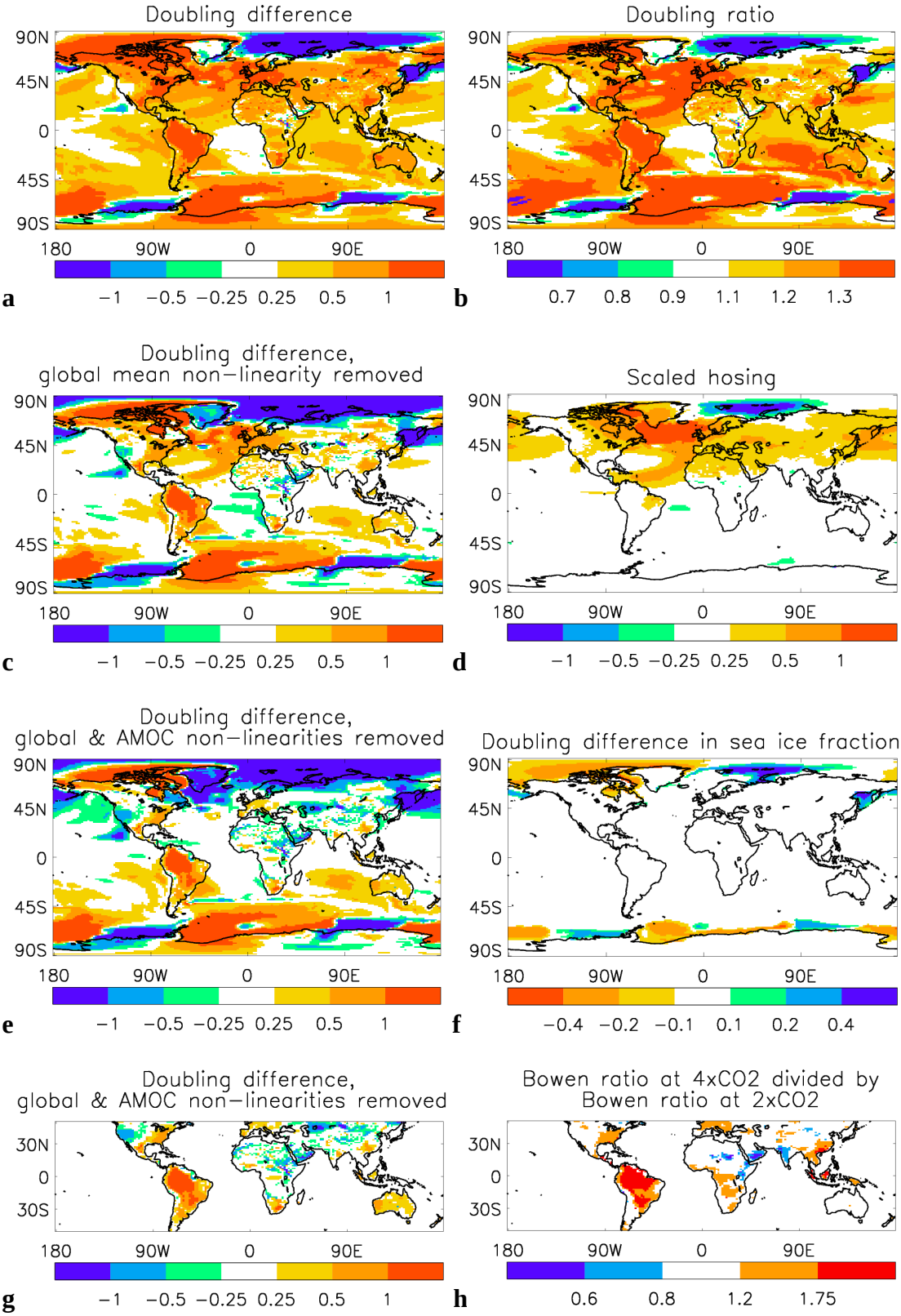

Figure 2. Mechanisms of nonlinear regional warming in HadGEM2-ES. Left column: doubling differences (K); a) unscaled; c) after global-mean nonlinearity is scaled out (Methods); e) as c), but with nonlinearity associated with the AMOC (panel d) subtracted; g) as e) but latitude range matches that of panel h). b) doubling ratio. d) estimated nonlinearity associated with the AMOC. f) doubling difference in sea ice

fraction. h) Bowen ratio at 4xCO_2 divided by Bowen ratio at 2xCO_2. All based on means over years 50-149 of the abrupt2xCO2, abrupt4xCO_2 or hosing experiments.

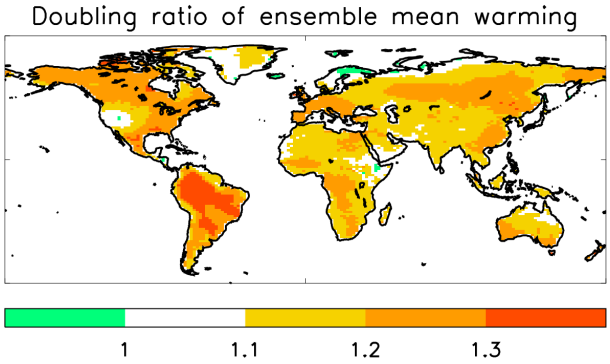

Figure 3. Doubling ratio of ensemble mean warming. Ensemble means are taken for each of the first and second CO_2 doublings first, then the doubling ratio calculated.

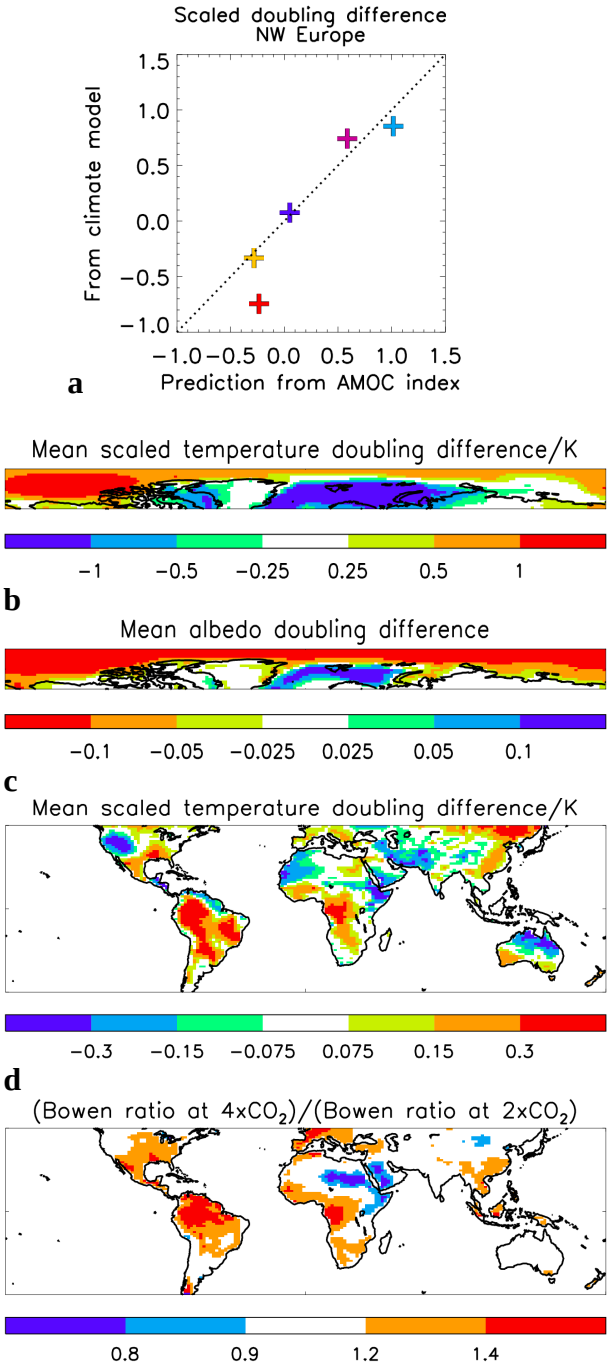

Figure 4. Multi-model mechanisms of temperature nonlinearity. All panels: 'scaled temperature doubling differences' have had the global mean nonlinearity scaled out**.** a) AMOC influence, averaged over NW Europe (land, 10W-20E, 45-70N). Y-axis: scaled temperature doubling difference for each model; x-axis: the HadGEM2-ES hosing temperature response scaled using the doubling difference in AMOC index for each model (as Figure 2d; Pink: HadGEM2-ES; dark blue: HadCM3; light blue: MIROC5; yellow: NCAR CESM1; red: IPSL CM5A-LR). b,c) Sea-ice influence. Ensemble means (excluding HadGEM2), of b: scaled temperature doubling difference and c: albedo doubling difference. d,e) Evaporation influence. d: Ensemble mean (excluding HadGEM2) scaled temperature doubling difference; e: Bowen ratio of

ensemble mean surface heat fluxes at $4xCO_2$, divided by the equivalent at $2xCO_2$ (as Figure 2h).

Supplementary material for 'Nonlinear regional warming at higher CO_2 concentrations'

Peter Good[1], Jason A. Lowe[1], Timothy Andrews[1], Andrew Wiltshire[1], Robin Chadwick[1], Jeff K Ridley[1], Matthew B Menary[1], Nathaelle Bouttes[2], Jean Louis Dufresne[3], Jonathan M Gregory[2,1], Nathalie Schaller[4,5], Hideo Shiogama[6]

[1] Met Office Hadley Centre, Exeter, United Kingdom

[2] NCAS-Climate, University of Reading, Reading, United Kingdom

[3] Laboratoire de Météorologie Dynamique, Institut Pierre Simon Laplace, Paris,France

[4] Institute for Atmospheric and Climate Science, Department of Environmental Sciences, Swiss Federal Institute of Technology, Zurich, Switzerland

[5] Atmospheric, Oceanic and Planetary Physics, University of Oxford, Parks Road, Oxford OX1 3PU, United Kingdom

[6] Climate Risk Assessment Section, Centre for Global Environmental Research, National Institute for Environmental Studies, Japan

To be submitted to Nature Climate Change

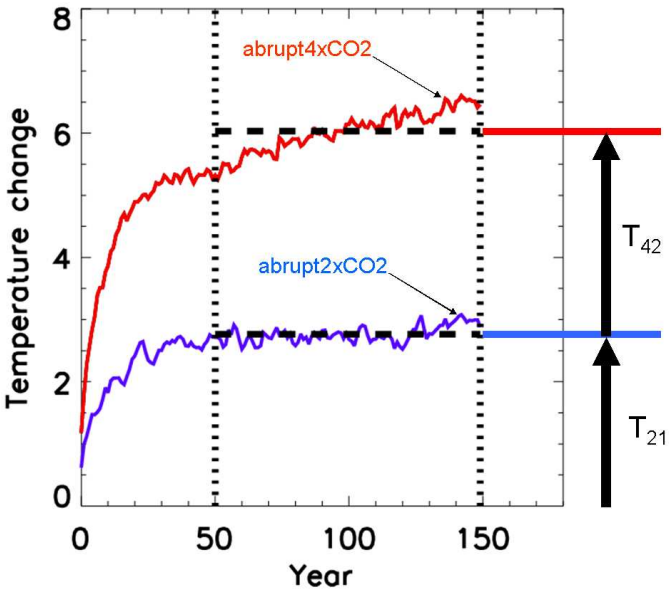

Supplementary Figure 1. Illustrating the doubling difference and doubling ratio calculations. The main results are averaged over years 50-149 – see vertical dotted lines. The red and blue curves show global mean warming timeseries for illustration. The doubling difference is given by $T_{42} - T_{21}$, the doubling ratio by T_{42} / T_{21}.

1. Interpreting averages over years 50-149 of the abruptCO2 experiments

Our analysis focuses on averages over years 50-149 of each abruptCO2 experiment. This section discusses how these results may approximately be related to policy-relevant scenario projections. This does not mean that the results are substitutes for scenario projections (in particular, the distinct effects of non-CO2 forcings are absent): it just gives a rough context. The main paper states that, "For abrupt2xCO2, these 100-year means may roughly be interpreted as the results for year 2100 of a CO2-only version of rcp4.5." This statement arises from the method behind Figure 1, as follows.

Supplementary Figure 2 shows the timeseries of global mean radiative forcing for rcp4.5 (blue). It also shows an idealised transient scenario (black line) that is roughly similar to rcp4.5. We show below that the mean over years 50-149 of the abrupt2xCO2 experiment represents an estimate of the response at year 2100 of the scenario represented by the black line.

As demonstrated in the main paper (Figures 1b,c) and in previous literature[1-3], it is possible to use a simple linear combination of abruptCO_2 responses to estimate climate change under a transient forcing experiment. This method works well (Figures 1b,c) when it is used to simulate periods in the transient experiment when the forcing matches that of the abruptCO_2 experiment.

The method we use to estimate the response to a transient experiment from an abruptCO2 experiment is a linear response function approach. It is given simply by the following equation:

$$y_i = \sum_{j=0}^{i} \frac{\Delta F_{i-j}}{\Delta F_a} x_j \qquad \text{supplementary equation 1}$$

where y_i is the estimated transient temperature response at year i and x_j is the temperature response at year j of the CO_2 step experiment. ΔF_{i-j} is the annual step change in radiative forcing during year i-j of the scenario. ΔF_a is the radiative forcing change in the abruptCO_2 experiment. (Essentially, this treats the transient scenario as a series of small annual step changes in forcing: the response to each step is estimated by scaling the abruptCO2 response).

The black line in Supplementary Figure 2 represents an experiment where CO2 is increased by 0.7% per year for 100 years, then held constant for 50 years (reaching a peak CO2 concentration of double the pre-industrial level). This corresponds to an approximately constant rate of forcing increase during the ramp-up period. As this experiment takes 100 years to double CO2, the annual change in forcing is equal to the abrupt2xCO2 forcing divided by 100. Therefore, the ratio $\Delta F_{i-j} / \Delta F_a$ is set equal to 1/100 for the first 100 years (i.e. for i-j <= 99 in supplementary equation 1); and equal to zero for the last 50 years (i.e. for i-j > 99). To obtain the warming at the end of the scenario, we set i=149 (the scenario is 150 years long). Therefore, $\Delta F_{i-j} / \Delta F_a$ is equal to 1/100 for j >= 50; and equal to zero for j < 50. Using supplementary

equation 1, therefore, the response at the end of this experiment may be estimated from the abrupt2xCO2 response as follows:

$$y = \sum_{j=50}^{149} \frac{1}{100} x_j^{(abrupt2xCO2)} \qquad \text{supplementary equation 2}$$

(The summation starts from j=50 because $\Delta F_{i-j} / \Delta F_a$ is zero for j < 50). This is simply equal to the mean over years 50-149 of the abrupt2xCO2 experiment – as used in the main paper.

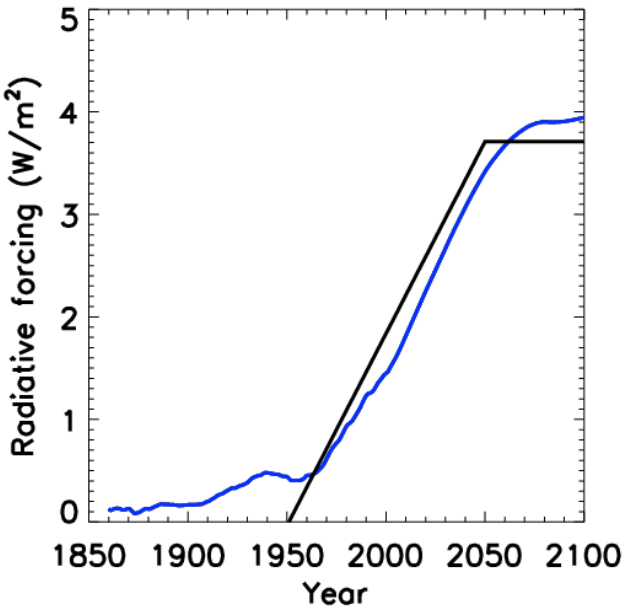

Supplementary Figure 2. Total global-mean radiative forcing timeseries. Blue: for rcp4.5, as estimated by the IAM used to produce the scenario forcing dataset[4] (from the RCP database: http://www.iiasa.ac.at/web-apps/tnt/RcpDb). Black: for a scenario where CO2 is increased by 0.7% per year for 100 years, then stabilised for 50 years.

1. Sea-ice non-linearity in HadGEM2-ES

The patterns of temperature nonlinearities over high latitude oceans (Figure 2e) correspond closely to nonlinearities in sea-ice cover (Figure 2f). The scale in Figure 2f is reversed, because reductions in sea-ice cover tend to drive increases in warming. Here we provide support for the nonlinear albedo feedback being a prominent driver of high-latitude temperature non-linearity..

Supplementary figure 3 shows statistics of the climatological mean and interannual variability in sea-ice fraction. The blue(red) lines show results when only regions with sea-ice doubling difference larger than 0.2(smaller than -0.2) are included. Climate means are shown for the control and each abruptCO2 experiment (panels a-c). Panel d shows the ratio in variability between the abrupt4xCO2 experiment and the control. Regions with positive nonlinearities in sea ice cover (with doubling difference > 0.2; c.f. Figure 2f) have intermediate ice cover in the control experiment (Supplementary figure 3a, blue line), but (near) zero ice cover in the abrupt4xCO_2 experiment (supplementary figure 3c, blue line). Correspondingly, the interannual variability in ice cover is much lower at 4xCO_2 than in the control (supplementary figure 3d, blue line). This is consistent with the idea of smaller albedo feedback at 4xCO_2 due to a transition from intermediate to negligible ice cover.

Regions with negative sea ice nonlinearities (doubling difference < -0.2) have much larger sea ice variability at 4xCO_2 than in the control (supplementary figure 3d, red line), and often have large ice cover in the control (supplementary figure 3a), and non-

zero cover even at 4xCO_2 (supplementary figure 3c). This is consistent with the idea of albedo feedback being higher in the abrupt4xCO_2 experiment.

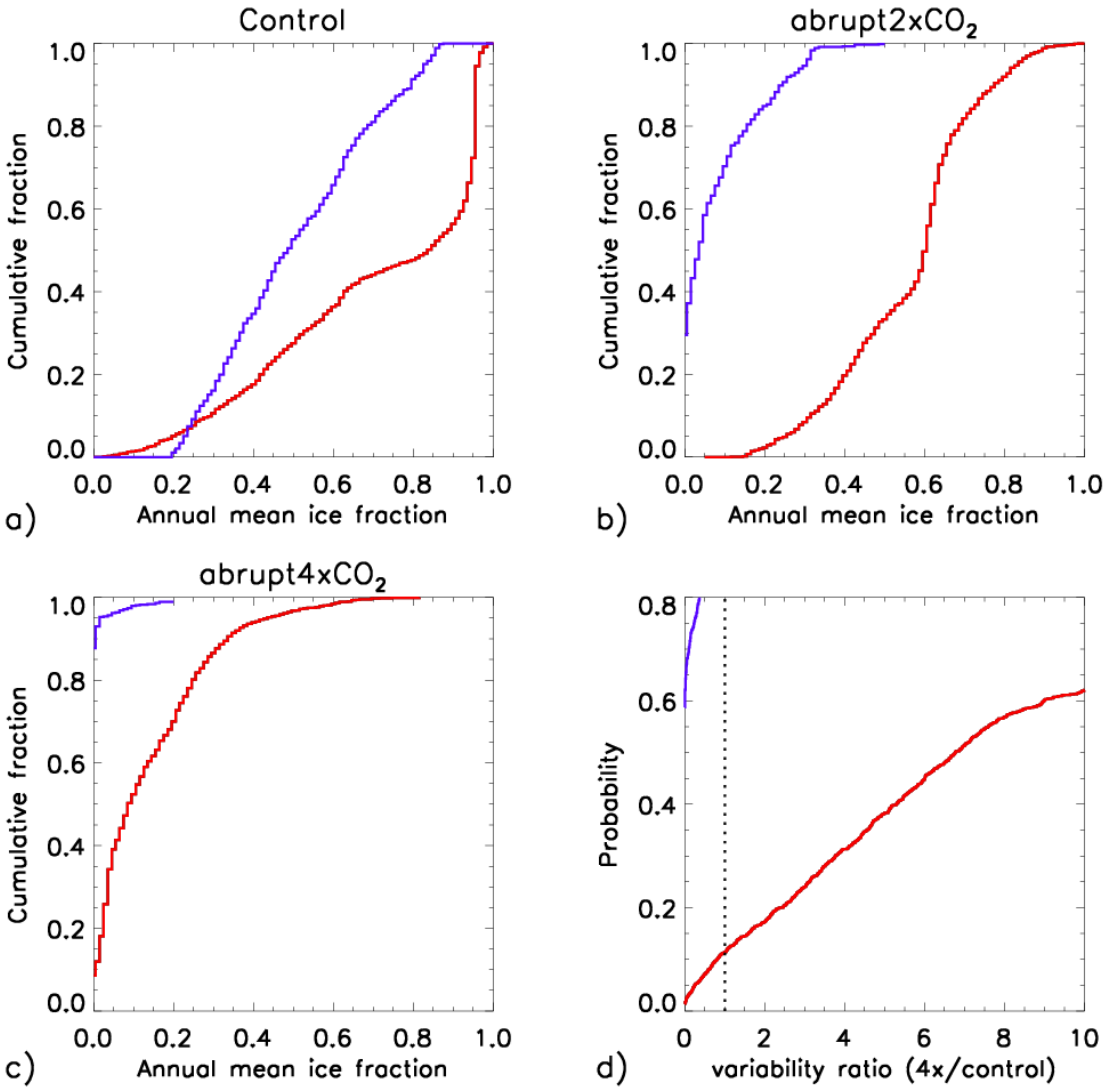

Supplementary figure 3. Statistics of sea-ice mean (a-c) and variability (d) for regions with (blue) sea-ice doubling difference > 0.2 and (red) sea-ice doubling difference < -0.2. Panel d) shows the ratio: (variability in abrupt4xCO_2)/(variability in control), where variability is quantified as the standard deviation in annual mean sea-ice cover over years 50-149 of each experiment.

2. Evaporation over the Amazon in HadGEM2-ES

The large temperature non-linearities over the Amazon are associated with a substantially larger Bowen ratio at $4xCO_2$ compared to $2xCO_2$ (Figure 2h). Here we link this to reduced forest tree stomatal conductance at higher CO_2, driven by a direct stomatal response to CO_2, with a secondary effect due to reduced photosynthesis at high temperature. We show results averaged over the western Amazon (72-60W, 12S-3N), capturing the main temperature non-linearity.

Over this region, latent heat flux from evaporation is significantly lower in the abrupt$4xCO_2$ experiment than in the abrupt$2xCO_2$ experiment (supplementary figure 4a; blue: abrupt$2xCO_2$; red: abrupt$4xCO_2$). The total turbulent heat flux is relatively similar in the two experiments (supplementary figure 4b), so the decrease in latent heat flux is balanced by a corresponding increase in sensible heat flux (supplementary figure 4c). This is consistent with the idea of restricted evaporation causing a larger proportion of surface heat to be lost by sensible heat, with a corresponding increase in surface temperature.

Surface evaporation is determined by atmospheric demand divided by net resistance[5]. The net resistance quantifies limitations on water supply, accounting for soil moisture, biophysical control by plants (via stomata) and the process of transferring moisture from the surface to the lowest atmospheric layer. The decrease in evaporation (at $4xCO_2$ compared to $2xCO_2$) is driven by a relatively large (around 35%) decrease in

1/(net resistance) – see Supplementary figure 4d. We plot 1/(net resistance), because evaporation is proportional to 1/(net resistance), at constant atmospheric demand. This decrease in 1/(net resistance) is dominated by a decrease in stomatal conductance associated with the broadleaf tropical forest trees: supplementary figure 4e shows changes due to stomatal conductance alone, and is similar to supplementary figure 4d.

The difference in stomatal conductance between the two experiments (seen in supplementary figure 4e) is largely due to a fast response of stomata to the different CO_2 levels. This appears in supplementary figure 4e as a difference between the red and blue lines present from the first year. Moisture stress is negligible for forest tress in this region in both experiments (not shown), so regional evaporation is independent of precipitation change.

The subsequent decline in conductance in the abrupt4xCO_2 experiment (supplementary figure 4e, red line) is driven in this model primarily by a decrease in photosynthesis, with stomata closing to maintain near constant leaf internal CO_2 concentration. Evidence for this is given in supplementary figure 4f. This shows that a near constant proportionality is maintained between stomatal conductance and gross primary productivity (GPP, a proxy for photosynthesis, as leaf area is almost constant in this region for these runs). The relationship between photosynthesis and stomatal conductance arises through the transport of carbon through a leaf, which is quantified by the following equation[6]:

$$A = \frac{g_s(c_c - c_i)}{1.6RT^*}$$

179 *A* is the leaf photosynthesis rate, g_s the stomatal conductance, $(c_c - c_i)$ is the CO_2
180 concentration gradient across the stomata, *R* the perfect gas constant and *T** the leaf
181 surface temperature in K (the latter is relatively constant in these runs as it is in units
182 of K). The near-constant proportionality between stomatal conductance and
183 photosynthesis (supplementary figure 4f, red line) means that $(c_c - c_i)$ is
184 approximately constant. That is, the model of stomatal conductance in HadGEM2-ES
185 acts to keep the internal leaf CO_2 concentration (c_i) roughly constant during the
186 abrupt4xCO_2 experiment (c_c, the external CO_2 concentration is approximately
187 constant during the abrupt4xCO_2 run). It does this by closing stomata (decreasing g_s),
188 which in turn reduces water loss.
189
190 Large uncertainties exist in the modelling of stomatal responses to CO2 increase[7].
191 HadGEM2-ES does not include photosynthetic acclimation[8], which could reduce the
192 decrease in GPP at high temperature, potentially reducing the decreases in stomatal
193 conductance. However, the magnitude of this effect is highly uncertain[9].
194
195

196

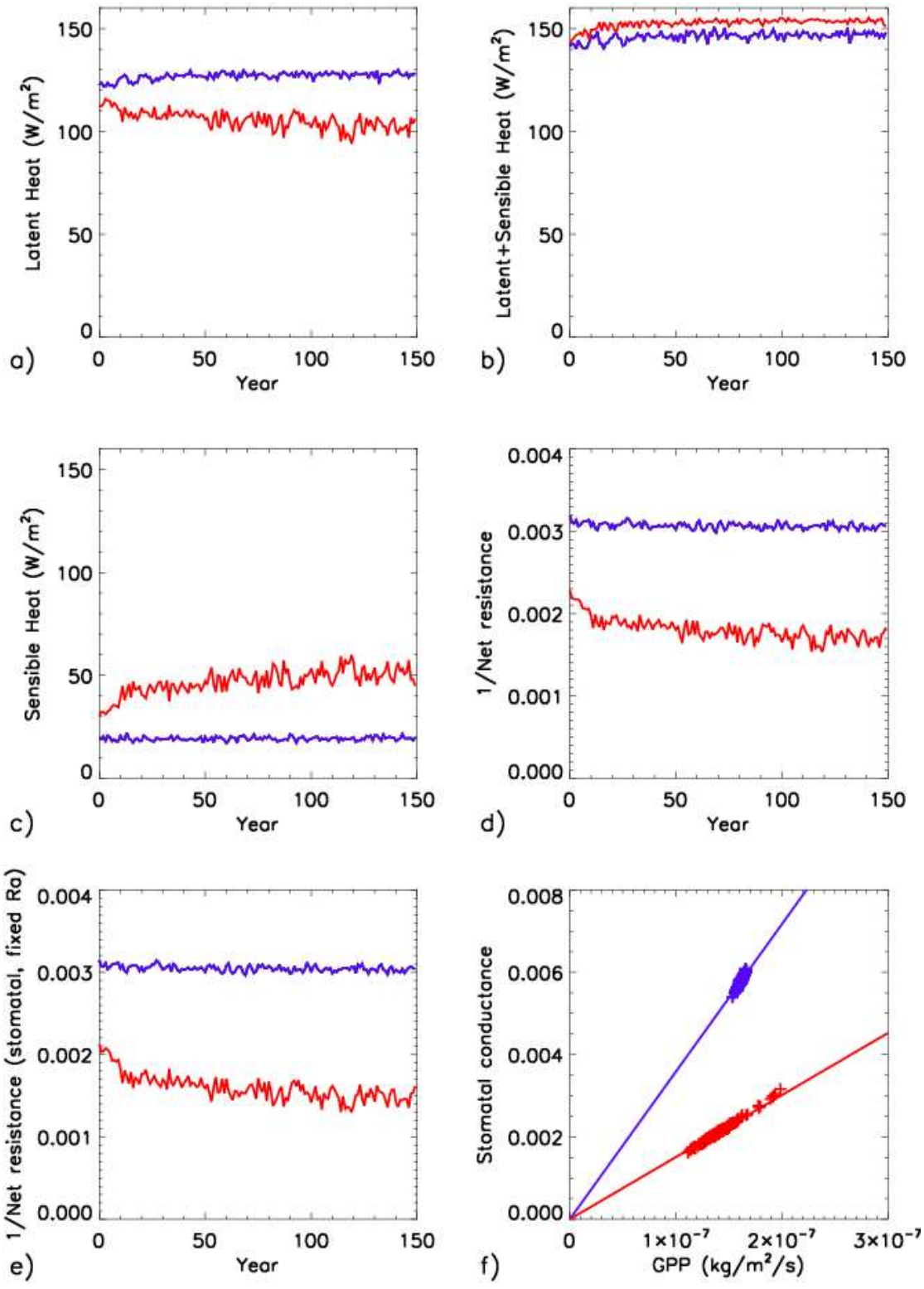

197

198 Supplementary figure 4. Diagnostics relating to evaporation, averaged over the

199 Western Amazon, for the abrupt2xCO_2 (blue) and abrupt4xCO_2 (red) experiments.

200 See text for description.

3. Multi-model statistics of nonlinearity over land

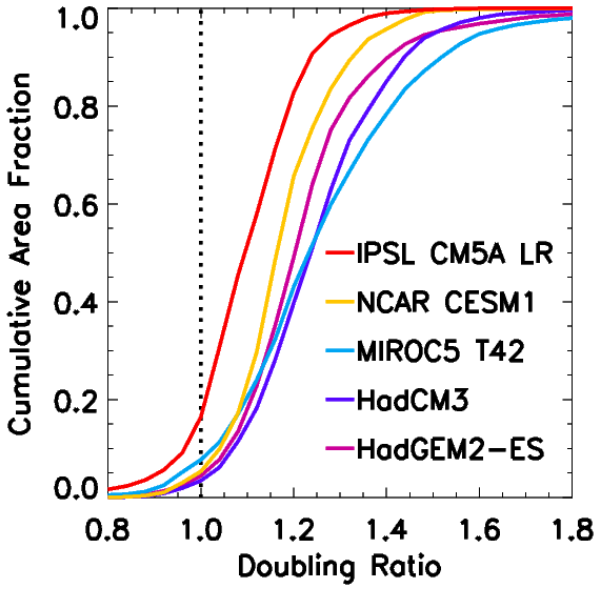

a)

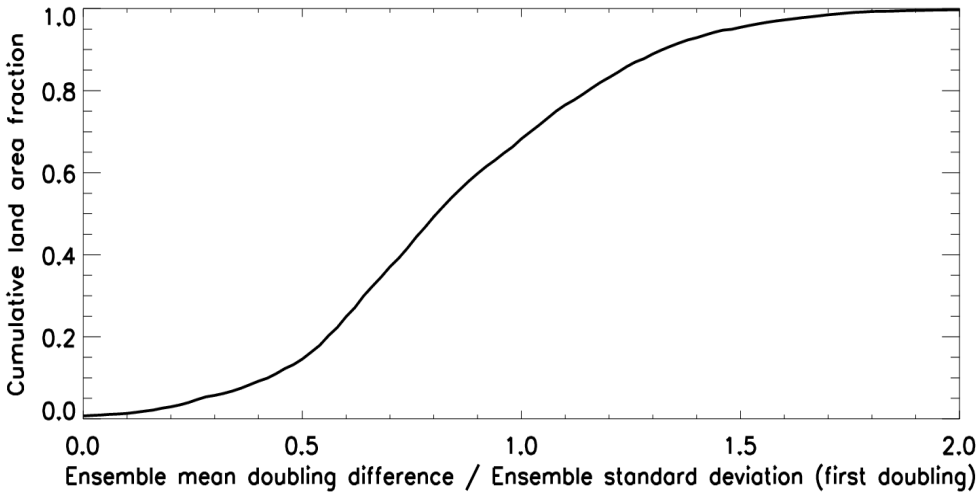

b)

Supplementary Figure 5. a) Cumulative area distribution functions of the temperature doubling ratio over land, for each model. b) Cumulative area distribution function of the ratio: (ensemble mean doubling difference) / (Ensemble standard deviation from the first doubling).

4. Inflation in model spread for the second CO_2 doubling

The main paper reports that, over about 30% of the land area, the model spread in warming per K of global warming is more than 1.4 times larger for the second doubling than for the first. In this section, we will address the possibility of the inflation of model spread being an artifact of internal variability.

A difference in the standard deviation between two datasets can arise simply from internal variability. This is because the climate state for each model is estimated from the mean over a finite period. Even though 100-year means are used in this study, internal variability may still play a role.

We denote the ratio between the standard deviation for the second doubling, and that for the first, as R:

$$R = \frac{\sigma_{42}}{\sigma_{21}},$$

where σ_{42}, the ensemble standard deviation for the second doubling (where CO2 changes from 2x to 4x pre-industrial levels) is given by:

$$\sigma_{42} = \sqrt{V_{42}^{(m)} + V_4^{(i)} + V_2^{(i)}},$$

where $V_{42}^{(m)}$ is the variance due to model differences alone; $V_4^{(i)}$ is the variance from internal variability in the climate at 4xCO2; and $V_2^{(i)}$ the equivalent at 2xCO2.

Similarly, σ_{21}, the standard deviation for the first doubling, is given by:

$$\sigma_{21} = \sqrt{V_{21}^{(m)} + V_2^{(i)} + V_1^{(i)}}$$

Therefore, R is given by:

$$R = \frac{\sqrt{V_{42}^{(m)} + V_4^{(i)} + V_2^{(i)}}}{\sqrt{V_{21}^{(m)} + V_2^{(i)} + V_1^{(i)}}}$$

$V_2^{(i)}$ appears on both top and bottom of this ratio. This means that if $V_2^{(i)}$ was much larger than the other variances, R would tend to 1 everywhere. This cannot explain our finding of large areas with R > 1.4.

If $V_4^{(i)}$ (the internal variability in the mean at 4xCO2) was increased, however, R would increase everywhere (and so the area with R > 1.4 would increase). We tested the importance of $V_4^{(i)}$ by artificially increasing it: by calculating the climate means for abrupt4xCO2 using shorter averaging periods (but centred on the same year as the 100-year means). This has minimal effect on our result: the fraction of land with R > 1.4 is still 32% even if this averaging period is reduced to 20 years (compared to 30% for 100 year means). This suggests that, for the 100-year means used in the main paper, internal variability has minimal effect on our estimate for the area with R > 1.4

5. Drivers of nonlinearity from individual models

The main paper (Figure 4) shows results for the albedo and evapotranspiration drivers averaged over the four additional climate models (NCAR-CESM1, IPSL CM5A-LR, MIROC5 T42 and HadCM3). Here we show results for individual models (Supplementary Figures 6,7). We also give doubling ratios for global-mean warming (Supplementary Table 1). The spread in the AMOC nonlinearity is illustrated in Figure 4a of the main paper.

As reported in the main paper, the patterns in albedo and evapotranspiration drivers show significant spread across the models. Therefore, their contribution to the overall uncertainty in warming for the second doubling may be substantial in the relevant regions (see discussion on how nonlinearity influences uncertainty in the main paper). The spread in the albedo driver (Supplementary Figure 6) may partly be associated with errors in simulated pre-industrial sea-ice cover (we show above that the sign of the nonlinearity is linked with the control sea-ice cover), so there may be potential for reducing uncertainty using observations. Similarly, the spread in the evapotranspiration driver (Supplementary Figure 7) may partly be associated with errors in pre-industrial soil moisture.

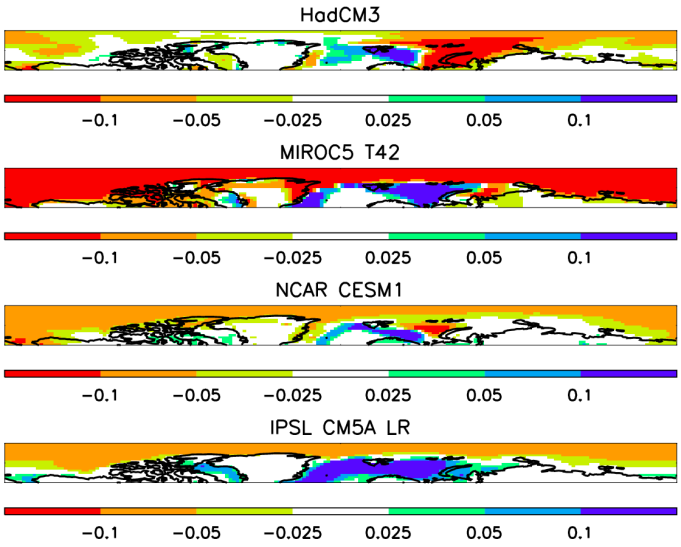

Supplementary Figure 6. Albedo doubling differences: as Figure 4c of the main paper, but for individual models.

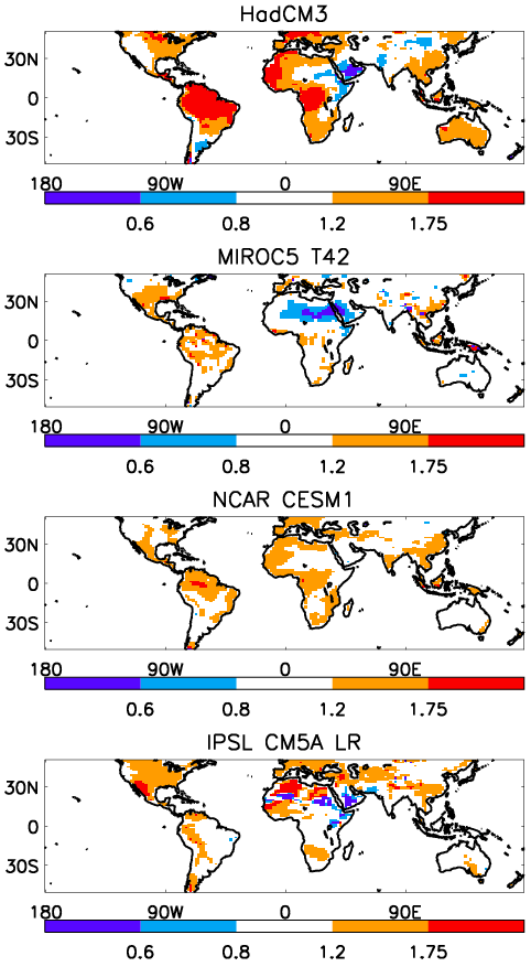

Supplementary Figure 7. Bowen ratio of ensemble mean surface heat fluxes at $4xCO_2$, divided by the equivalent at $2xCO_2$: as Figure 4e but for each model.

Model	Doubling ratio in global mean warming
NCAR CESM1	1.21
IPSL CM5A-LR	1.05
MIROC5 T42	1.27
HadCM3	1.19
HadGEM2-ES	1.18

Supplementary Table 1. Doubling ratio in global-mean warming for each model.

5. Model descriptions

Model and citation	Resolution	Citation
NCAR CESM1[10]	0.9° longitude x 1.25° latitude, 26 vertical levels	Gent et al., 2011
IPSL CM5A-LR[11]	3.75° longitude x 1.875° latitude, 39 vertical levels	Dufresne et al., 2013
MIROC5 T42[12]	T42, 40 vertical levels	Watanabe et al., 2010
HadCM3[13,14]	3.75° longitude x 2.5° latitude, 19 vertical levels	Gordon et al., 2000, Pope et al., 2000

Supplementary Table 2. Descriptions of models used (HadGEM2-ES is described in Methods of main text).

References

1 Good, P., Gregory, J. M. & Lowe, J. A. A step-response simple climate model to reconstruct and interpret AOGCM projections. *Geophysical Research Letters* **38**, -, doi:Artn L01703 Doi 10.1029/2010gl045208 (2011).

2 Good, P., Gregory, J. M., Lowe, J. A. & Andrews, T. Abrupt CO2 experiments as tools for predicting and understanding CMIP5 representative concentration pathway projections. *Climate Dynamics* **40**, 1041-1053, doi:DOI 10.1007/s00382-012-1410-4 (2013).

3 Chadwick, R., Wu, P. L., Good, P. & Andrews, T. Asymmetries in tropical rainfall and circulation patterns in idealised CO2 removal experiments. *Climate Dynamics* **40**, 295-316, doi:DOI 10.1007/s00382-012-1287-2 (2013).

4 Meinshausen, M. *et al.* The RCP greenhouse gas concentrations and their extensions from 1765 to 2300. *Climatic Change* **109**, 213-241, doi:DOI 10.1007/s10584-011-0156-z (2011).

5 Seneviratne, S. I. *et al.* Investigating soil moisture-climate interactions in a changing climate: A review. *Earth-Sci Rev* **99**, 125-161, doi:DOI 10.1016/j.earscirev.2010.02.004 (2010).

6 Cox, P. M. Description of the TRIFFID Dynamic Global Vegetation Model. *Technical Note 24, Hadley Centre, Met Office*, 17 pp. (2001).

7 Rammig, A. *et al.* Estimating the risk of Amazonian forest dieback. *New Phytol* **187**, 694-706, doi:DOI 10.1111/j.1469-8137.2010.03318.x (2010).

8 Berry, J. A. & Bjorkman, O. Photosynthetic response and adaptation to temperature in higher plants. *Annual Review of Plant Physiology* **31**, 491-543 (1980).

9 Smith, N. G. & Dukes, J. S. Plant respiration and photosynthesis in global-scale models: incorporating acclimation to temperature and CO2. *Glob Change Biol* **19**, 45-63, doi:DOI 10.1111/j.1365-2486.2012.02797.x (2013).

10 Gent, P. R. *et al.* The Community Climate System Model Version 4. *Journal of Climate* **24**, 4973-4991, doi:Doi 10.1175/2011jcli4083.1 (2011).

11 Dufresne, J. L. *et al.* Climate change projections using the IPSL-CM5 Earth System Model: from CMIP3 to CMIP5. *Climate Dynamics* **40**, 2123-2165, doi:DOI 10.1007/s00382-012-1636-1 (2013).

12 Watanabe, M. *et al.* Improved Climate Simulation by MIROC5. Mean States, Variability, and Climate Sensitivity. *Journal of Climate* **23**, 6312-6335, doi:Doi 10.1175/2010jcli3679.1 (2010).

13 Gordon, C. *et al.* The simulation of SST, sea ice extents and ocean heat transports in a version of the Hadley Centre coupled model without flux adjustments. *Climate Dynamics* **16**, 147-168 (2000).

14 Pope, V. D., Gallani, M. L., Rowntree, P. R. & Stratton, R. A. The impact of new physical parametrizations in the Hadley Centre climate model: HadAM3. *Climate Dynamics* **16**, 123-146 (2000).

342